LIGHT-EMITTING DIODES

SECOND EDITION

E. FRED SCHUBERT

Rensselaer Polytechnic Institute,
Troy, New York

CAMBRIDGE
UNIVERSITY PRESS

SAMSUNG EX. 1031 - 1/30

CAMBRIDGE UNIVERSITY PRESS
Cambridge, New York, Melbourne, Madrid, Cape Town, Singapore, São Paulo,
Delhi, Dubai, Tokyo, Mexico City

Cambridge University Press
The Edinburgh Building, Cambridge CB2 8RU, UK

Published in the United States of America by Cambridge University Press, New York

www.cambridge.org
Information on this title: www.cambridge.org/9780521865388

First edition © E. Fred Schubert 2003
Second edition © E. Fred Schubert 2006

This publication is in copyright. Subject to statutory exception
and to the provisions of relevant collective licensing agreements,
no reproduction of any part may take place without
the written permission of Cambridge University Press.

First edition published 2003
Second edition 2006
Second edition reprinted 2007
4th printing 2010

Printed in the United Kingdom at the University Press, Cambridge

A catalog record for this publication is available from the British Library

ISBN 978-0-521-86538-8 Hardback

Cambridge University Press has no responsibility for the persistence or accuracy of URLs for external or third-party internet websites referred to in this publication, and does not guarantee that any content on such websites is, or will remain, accurate or appropriate.

This material may be protected by Copyright law (Title 17 U.S. Code)

10

Reflectors

Ideal reflectors incorporated into a device structure should have (*i*) high reflectivity, (*ii*) a sufficiently broad spectral range of the high-reflectivity band, (*iii*) omnidirectional characteristics, and (*iv*) low resistivity (provided current flows through the reflector). It is a question of great practical and intellectual interest what type of reflector best meets these multiple requirements.

Different types of reflectors are shown in Fig. 10.1 including a metallic reflector, distributed Bragg reflector (DBR), hybrid metal–DBR, reflectors based on total internal reflection (TIR), and an omni-directional reflector. The characteristics of the different types of reflectors will be discussed below.

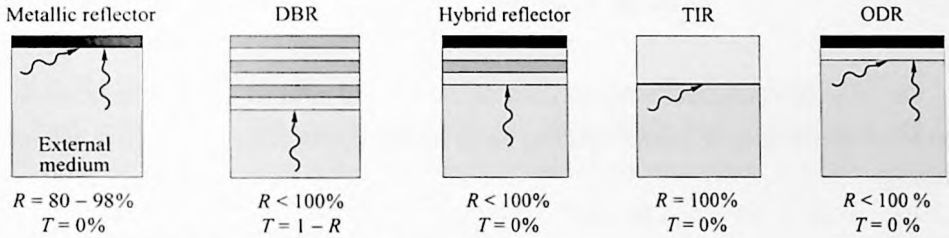

Fig. 10.1. Different types of reflectors including metallic reflector, distributed Bragg reflector (DBR), hybrid reflector, total internal reflector (TIR), and a triple-layer omni-directional reflector (ODR). Also given are angles of incidence for high reflectivity and typical reflectances and transmittances.

An ***external medium*** is indicated in the figure. In an LED structure with a reflector, the external medium is a semiconductor. The external medium has a significant influence on the reflector properties. For example, the reflectivity of a metal–semiconductor reflector is lower compared to a metal–air reflector.

SAMSUNG EX. 1031 - 3/30

10.1 Metallic reflectors, reflective contacts, and transparent contacts

Having been used by humankind for several millenniums, metal–air reflectors are the oldest type of reflector with high reflectivity. Metal reflectors are characterized by a broad spectral reflectivity band and a weak angular dependence of the reflectivity. The first high-quality metallic reflectors were used in reflection telescopes for astronomy applications (Bell, 1922).

An experimental reflectance spectrum of a silver–air reflector at normal incidence is shown in Fig. 10.2. The reflectance spectrum is characterized by a broad spectral band of high reflectivity and an average reflectance of 98.5%.

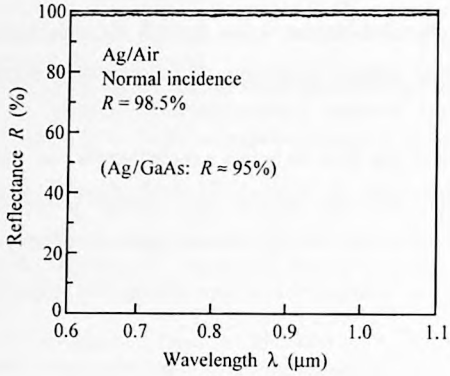

Fig. 10.2. Measured reflectance of a silver/air reflector for normal incidence. The average reflectivity in the visible spectrum is 98.5%.

The reflectance (amplitude reflection coefficient) of a metal reflector and an external medium can be calculated from the Fresnel equation, which for media with complex refractive indices is given by

$$r = \frac{\mathcal{E}_r}{\mathcal{E}_i} = \frac{\overline{N}_1 - \overline{N}_2}{\overline{N}_1 + \overline{N}_2} \tag{10.1}$$

where $\overline{N}_1$ and $\overline{N}_2$ are the complex refractive indices of the two media.

The reflected and transmitted *intensities* are proportional to the square of the electric field. The ***reflectivity*** or ***reflectance*** (power reflection coefficient) is given by

$$R = \frac{|\mathcal{E}_r|^2}{|\mathcal{E}_i|^2} = |r|^2 = \left|\frac{\overline{N}_1 - \overline{N}_2}{\overline{N}_1 + \overline{N}_2}\right|^2 = \frac{|\overline{N}_1 - \overline{N}_2|^2}{|\overline{N}_1 + \overline{N}_2|^2} \tag{10.2}$$

SAMSUNG EX. 1031 - 4/30

The energy conservation law requires that the power transmission coefficient in a lossless reflector is given by

$$T = 1 - R \,. \tag{10.3}$$

Metals are lossy media so that the transmittance $T \approx 0$ for thick metal films. The Fresnel equation can be used to calculate the reflectance of a metal–dielectric interface. Assuming that the complex refractive indices of the dielectric and the metal are $\bar{N}_1 = \bar{n}_1$ and $\bar{N}_2 = \bar{n}_2 + \mathrm{i}\bar{k}_2$, respectively, the reflectance is given by

$$r = \frac{\bar{n}_1 - (\bar{n}_2 + \mathrm{i}\,\bar{k}_2)}{\bar{n}_1 + (\bar{n}_2 + \mathrm{i}\bar{k}_2)} \quad \text{and} \quad \boxed{R = \frac{(\bar{n}_1 - \bar{n}_2)^2 + \bar{k}_2^{\,2}}{(\bar{n}_1 + \bar{n}_2)^2 + \bar{k}_2^{\,2}}} \,. \tag{10.4}$$

An ideal metal has very high conductivity, i.e. $\sigma \to \infty$ and therefore $\bar{k} \to \infty$. (Note that conductivity σ and the imaginary part of the refractive index $\bar{k}$ are related by $\sigma = 2\bar{n}\omega\varepsilon_0\bar{k}$. Also note that the absorption constant α and the imaginary part of the refractive index are related by $\alpha = 4\pi\bar{k}/\lambda_0$.) We thus obtain for an ideal metal

$$|r| \approx 1, \qquad R \approx 1, \qquad \text{and} \qquad \phi_r = \pi \,. \tag{10.5}$$

That is, the ideal metal has a unit reflection coefficient, unit reflectance, and a phase shift of π.

Real metals have high conductivity (but not an infinitely high conductivity) and the reflectivity of any real metal is therefore less than unity. Loss mechanisms in metals were first analyzed in terms of the Drude model (Drude, 1904). Table 10.1 gives the $\bar{n}$ and $\bar{k}$ values of several metals and semiconductors.

Table 10.1. Real and imaginary part of the refractive index for different semiconductors and metals at 0.5 and 1.0 μm.

Material	GaP	GaP	Si	Ag	Ag	Au	Au	Al	Al
$\lambda =$	0.5 μm	1.0 μm	1.0 μm	0.5 μm	1.0 μm	0.5 μm	1.0 μm	0.5 μm	1.0 μm
$\bar{n}$	3.5	3.1	3.6	0.05	0.04	0.86	0.26	0.77	1.35
$\bar{k}$	≈ 0	≈ 0	≈ 0	3.1	7.1	1.90	6.82	6.08	10.7

Using Eq. (10.4), the reflectance of a metal–air and metal–semiconductor boundary can be calculated; the results are given in Table 10.2. Inspection of the table reveals that the visible-

SAMSUNG EX. 1031 - 5/30

spectrum reflectivity is generally lower for metal-semiconductor interfaces than that of metal-air interfaces. This is due to the lower refractive-index contrast of the metal-semiconductor boundary.

Table 10.2. Calculated reflectivity of metal–air and metal–semiconductor reflectors at 0.5 and 1.0 μm.

Material	R (%)	Material	R (%)	Material	R (%)
Ag/air (0.5 μm)	0.982	Al/air (0.5 μm)	0.923	Au/air (0.5 μm)	0.514
Ag/air (1.0 μm)	0.997	Al/air (1.0 μm)	0.955	Au/air (1.0 μm)	0.979
Ag/GaP (0.5 μm)	0.969	Al/GaP (0.5 μm)	0.805	Au/GaP (0.5 μm)	0.470
Ag/GaP (1.0 μm)	0.992	Al/GaP (1.0 μm)	0.876	Au/GaP (1.0 μm)	0.945
Ag/Si (1.0 μm)	0.991	Al/Si (1.0 μm)	0.861	Au/Si (1.0 μm)	0.939

Although metals are simple and viable reflectors, the reflection losses or ***mirror losses*** are quite high. The loss of one reflection event, $(1 - R)$, is about 5% for metal-semiconductor reflectors. Losses are particularly high for waveguided modes shown in Fig. 10.3. The intensity of waveguided modes decays according to

$$I/I_0 = R^N = (1-L)^N \approx 1 - NL \tag{10.6}$$

where N is the number of reflection events, and the mirror loss is $L = 1 - R$ ($L << 1.0$ and $R \approx 1.0$). The equation illustrates that a small difference (e.g. a few percent) in R can make a large difference (e.g. a factor of 2) in the intensity of waveguided modes after N reflection events.

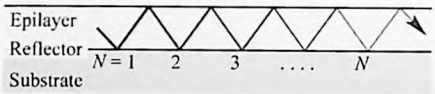

Fig. 10.3. Attenuation of waveguide mode due to lossy reflector.

Metal–semiconductor reflectors have been used in AlGaInP LEDs by Horng *et al.* (1999a, 1999b) to increase the light-extraction efficiency. The layer sequence of the finished device consisted of AlGaInP/AuBe/SiO_2/Si. The p-type AlGaInP–AuBe interface served as a reflector and as a broad-area ohmic contact. The AuBe layer also served as a supply layer for Be acceptors to attain low contact resistance. The contacts were annealed at 450 °C for 15 minutes. The LEDs were fabricated by a wafer-bonding process using a Si substrate. After the bonding process, the

SAMSUNG EX. 1031 - 6/30

GaAs substrate, on which the epitaxial layers had been grown, was removed. Si has a higher thermal conductivity than GaAs thus allowing for lower junction temperatures and reducing the joule-heating-induced emission-wavelength shift. The emission from the metal-reflector AlGaInP LEDs exceeded those of reference LEDs with DBRs fabricated on GaAs substrates.

Annealing and alloying forms low-resistance ohmic contacts. Typical annealing temperatures for alloyed contacts are between 375 and 450 °C for III–V arsenides and III–V phosphides and up to 600 °C for III–V nitrides. During the annealing process, the metal surface changes from smooth to rough and a concomitant decrease in the optical reflectivity results.

In contrast, non-alloyed contacts are just deposited on the semiconductor without annealing. Highly doped semiconductor surface layers are needed to obtain good ohmic *I–V* characteristics for such non-alloyed ohmic contacts. However, even for highly doped semiconductors, the contact resistance of non-alloyed contacts is usually higher than for alloyed contacts.

Thick metallic reflectors and hybrid reflectors are absorbing reflectors that should not be used as light-exit reflectors in LEDs and vertical-cavity surface emitting lasers. Metal contacts become practically opaque for thicknesses > 50 nm. That is, the transmittance of hybrid reflectors is near zero, unless the thickness of the metal is very thin (Tu *et al.*, 1990).

Very thin metal contacts are semi-transparent. Most metal contacts have a transmittance of approximately 50% at a metal film thickness of 5–10 nm. The exact value of the transmittance needs to be calculated by taking into account the real and imaginary part of the refractive index (see, for example, Palik, 1998). However, very thin metallic contacts may form an islanded structure rather than a single continuous film. Furthermore, the electrical resistance of thin metal films can be large, in particular if an islanded structure is formed.

In LEDs with transparent substrates, e.g. AlGaInP LEDs on GaP, light emanating from the active region is incident on the substrate contact. To increase the reflectance of the backside, an ohmic contact geometry covering only a small fraction of the substrate surface can be used, such as a multiple-stripe or a ring-shaped contact. Using Ag-loaded conductive epoxy to attach the LED die to the package provides a high-reflectivity material in the regions not covered by the ohmic contact.

The die-attach epoxy can also serve as a reflector in LEDs grown on a transparent material, e.g. GaInN LEDs grown on sapphire substrates. Conductive Ag-loaded epoxy has a high conductivity as well as high reflectance. Such a highly reflective epoxy can increase the extraction efficiency in LEDs grown on transparent substrates.

There are ohmic contacts that are transparent to visible light. Such ***transparent ohmic***

SAMSUNG EX. 1031 - 7/30

contacts include indium tin oxide, frequently referred to as ITO (Ray *et al.*, 1983; Sheu *et al.*, 1998; Margalith *et al.*, 1999; Mergel *et al.*, 2000; Shin *et al.*, 2001). The material can be considered as a tin oxide semiconductor that is doped with indium. Indium substitutes for tin and therefore acts as an acceptor. Generally the specific contact resistance of ITO contacts is higher than the contact resistance of alloyed metal contacts.

10.2 Total internal reflectors

Total internal reflection is a fascinating phenomenon occurring at the boundary between two dielectric media with different refractive indices. Total internal reflection was first discovered by Johannes Kepler in the early 1600s (Kepler, 1611). Kepler attempted to explain the apparent bending of objects partially submersed in water. Kepler discovered that for rays near normal incidence, the ratio of the angles of incidence and refraction is proportional to the ratio of what are now known as the refractive indices of the media. Kepler's relationship can be expressed as

$$\bar{n}_1 \theta_1 = \bar{n}_2 \theta_2 \tag{10.7}$$

where the angles θ_1 and θ_2 are measured with respect to the surface normal. Comparison with the law discovered between 1621 and 1625 by Cornelius Willebrord Snell (***Snell's law***)

$$\boxed{\bar{n}_1 \sin\theta_1 = \bar{n}_2 \sin\theta_2} \tag{10.8}$$

reveals that Kepler found the small-angle approximation of Snell's law. The angles used in Snell's law are shown in Fig. 10.4.

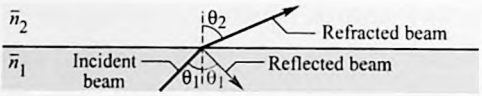

Fig. 10.4. Reflected and refracted light ray at the boundary between two media with refractive indices $\bar{n}_1$ and $\bar{n}_2$, where $\bar{n}_1 > \bar{n}_2$.

Kepler also discovered that, with suitable materials and sufficiently shallow angles of incidence, the refracted angle can be made to exceed 90°, resulting in total internal reflection. The critical angle for total internal reflection can be derived from Snell's law using the condition $\theta_2 = 90°$. Hence

$$\theta_{1,\mathrm{crit}} = \arcsin(\bar{n}_2 / \bar{n}_1) \,. \tag{10.9}$$

SAMSUNG EX. 1031 - 8/30

Because the ratio of the refractive indices on the right-hand side of the equation, $\bar{n}_2 / \bar{n}_1$, must be ≤ 1.0, total internal reflection can occur only in the optically denser material. Total internal reflection occurs for all angles of incidence $\theta_1 > \theta_{1,\text{crit}}$. For grazing angles of incidence and a sufficiently high index contrast, a light ray cannot leave a medium of high refractive index.

Isaac Newton later showed that, for most transparent media, the refractive index could be taken as unity plus a term proportional to the medium's mass density (measured in units of g/cm^3). Media with high refractive index are therefore frequently called ***optically dense*** materials.

The most fascinating application of total internal reflection is fiber optic communication in which light rays, by undergoing total internal reflection events, are guided over thousands of kilometers in the core of a silica fiber. In 1841, the guiding of light was first demonstrated by Daniel Colladon using a jet of water as the high-index material (Hecht, 2001). This phenomenon is used to the present day to enhance the appearance of water fountains at night. The apparatus built by Daniel Colladon, who is considered the father of light guiding, is shown in Fig. 10.5.

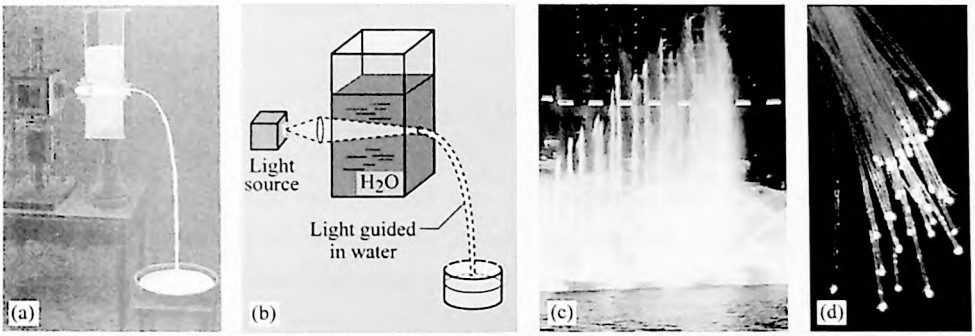

Fig. 10.5. (a) Historical drawing and (b) schematic illustration of apparatus used in 1841 by Swiss engineer Daniel Colladon to demonstrate the guiding of light by total internal reflection in a jet of water. (c) Light guiding used to beautify appearance of fountain in Las Vegas, Nevada. (d) Fiber-optic strands (after The Free Dictionary.com, 2005).

In light-emitting devices based on semiconductors, total internal reflection represents a major problem as it hinders the out-coupling of light out of the semiconductor die. As semiconductors have a large refractive index of typically 2.0–3.5, the critical angle for total internal reflection is small. Whereas the problem is severe for III–V arsenides and phosphides ($\bar{n} \approx 3.0$) it is less severe for III–V nitrides ($\bar{n} \approx 2.0$). Total internal reflection is of little concern in *organic* light-

SAMSUNG EX. 1031 - 9/30

emitting diodes due to the low refractive indices of organic materials.

One of the unique features of total internal reflection is that the magnitude of the reflection is $R = 1.0$ ("total"). This enables the demonstration of reflectors with zero mirror loss, a feature that has been employed advantageously in lasers. Edge-emitting lasers (Smith *et al.*, 1993) as well as microdisk lasers ("whispering gallery lasers") (McCall *et al.*, 1992) have employed total internal reflection to demonstrate cavities with very high cavity-quality factors.

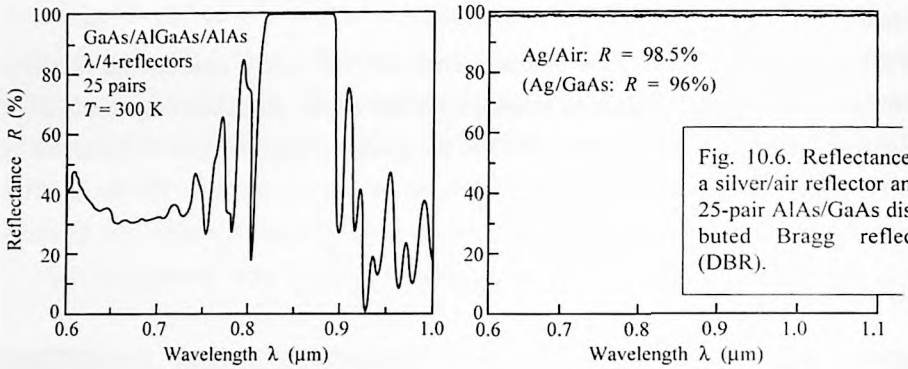

Fig. 10.6. Reflectance of a silver/air reflector and a 25-pair AlAs/GaAs distributed Bragg reflector (DBR).

10.3 Distributed Bragg reflectors

The reflectance spectra of a metal mirror and a DBR are compared in Fig. 10.6. Whereas metal reflectors exhibit a broad band with high reflectivity, DBRs display only a narrow band of high reflectivity denoted as the ***stop band***. However, while the metal reflector has a certain reflectivity, the DBR's reflectivity can be increased by increasing the number of reflector pairs so long as these reflector pairs are fully transparent.

For LED structures on light-absorbing substrates, about 50% of the light emitted by the active region is absorbed by the substrate. This represents a substantial loss. The absorption of light in the substrate can be avoided by placing a reflector between the substrate and the LED active layers. Light emanating from the active region towards the substrate will then be reflected and can escape from the semiconductor through the top surface.

Distributed Bragg reflectors (DBRs) are well suited for inclusion between the substrate and the active layers. The schematic LED structure with a DBR is shown in Fig. 10.7. LEDs with DBRs were first demonstrated by Kato *et al.* (1991) in the AlGaAs/GaAs material system. The LED had a 25-pair AlAs/GaAs or AlGaAs/GaAs DBR and emitted in the infrared at 870 nm.

SAMSUNG EX. 1031 - 10/30

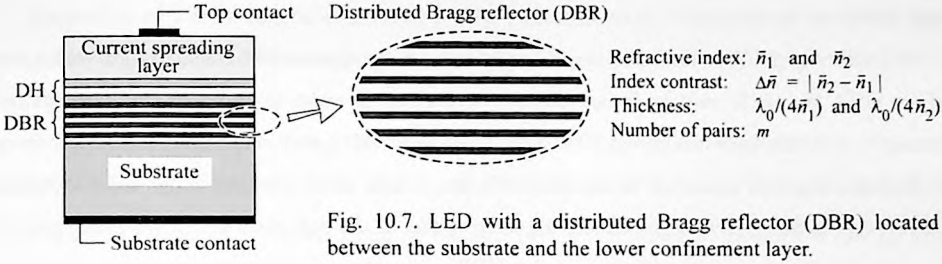

Fig. 10.7. LED with a distributed Bragg reflector (DBR) located between the substrate and the lower confinement layer.

A DBR is a multi-layer reflector consisting of typically 5–50 pairs of two materials with different refractive indices. As a result of the difference in refractive index, Fresnel reflection occurs at each of the interfaces. Usually the refractive index difference between the two materials is small so that the magnitude of the Fresnel reflection at one interface is also quite small. However, DBRs consist of many interfaces. More importantly, the thicknesses of the two materials are chosen in such a way that *all reflected waves* are in *constructive interference*. For normal incidence, this condition is fulfilled when both materials have a thickness of a *quarter wavelength* of the light, i.e.

$$t_{l,h} = \lambda_{l,h}/4 = \lambda_0/(4\,\bar{n}_{l,h}) \qquad \text{(normal incidence)} \qquad (10.10)$$

where λ_0 is the vacuum Bragg wavelength of the light, $t_{l,h}$ is the thickness of the low-index (l) and high-index (h) material, and $\bar{n}_{l,h}$ is the refractive index of the low-index (l) and high-index (h) material. The thickness of $t_{l,h}$ given in Eq. (10.10) can be not only $\lambda/4$, but also an odd-numbered integer multiple of $\lambda/4$, i.e. $3\lambda/4$, $5\lambda/4$, $7\lambda/4$, and so on. These thicknesses will also result in constructive interference of the reflected waves. For layer thicknesses greater than $\lambda/4$, e.g. $3\lambda/4$, the reflector will, however, have a narrower high-reflectivity stop band.

For an oblique angle of incidence, the wave vector can be separated into a parallel and a normal component. As in the normal-incident case, the thickness of the DBR layers must be a quarter wavelength for the wave vector component normal to the DBR layers. For an oblique angle of incidence $\Theta_{l,h}$, the optimum thicknesses for high reflectivity are given by

$$t_{l,h} = \lambda_{l,h}/(4\cos\Theta_{l,h}) = \lambda_0/(4\,\bar{n}_{l,h}\cos\Theta_{l,h}) \qquad \text{(oblique incidence)}\,. \qquad (10.11)$$

Again, the thickness $t_{l,h}$ given in Eq. (10.11) can also be an odd-numbered integer multiple of the value given by the equation. For DBRs with sufficiently many quarter-wave pairs, reflectivities

SAMSUNG EX. 1031 - 11/30

near 100% can be obtained.

A DBR must fulfill several additional conditions. Firstly, since a DH is usually grown on top of the DBR, the DBR must be lattice matched to the DH in order to avoid misfit dislocations. Secondly, to attain high-reflectivity DBRs, the constituent DBR materials need to be transparent at the wavelength of operation unless the DBR has a high index contrast. High index-contrast DBRs (e.g. Si/SiO_2) yield high reflectivity, even if one of the materials is weakly absorbing at the wavelength of interest. Thirdly, if the DBR is in the current path, the DBR must be conductive.

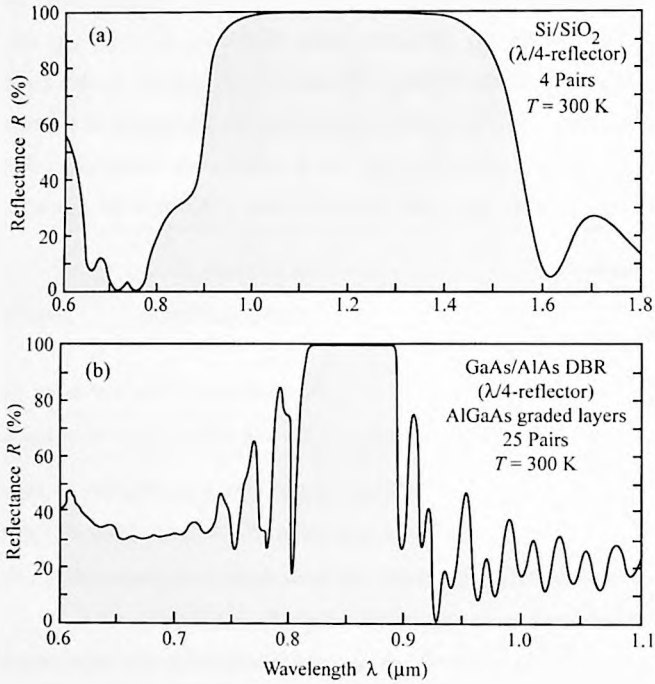

Fig. 10.8. Reflectance of two distributed Bragg reflectors (DBRs) versus wavelength. (a) Four-pair Si/SiO_2 reflector with high index contrast. (b) 25-pair AlAs/GaAs reflector. The high-index-contrast DBR only needs four pairs to attain high reflectivity. Note that the stop band of the high-index-contrast DBR is wider compared with the low-contrast DBR.

The reflectances of a Si/SiO_2 and an AlAs/GaAs DBR versus wavelength are shown in Fig. 10.8. The Bragg wavelength is located in the center of the high-reflectivity band or ***stop band***. Inspection of the figure reveals that (*i*) the reflectivity of high-contrast DBRs (Si/SiO_2) is much higher than the reflectivity of low-index-contrast DBRs (AlAs/GaAs) for the same number of quarter-wave pairs and that (*ii*) the width of the stop band of the high-index-difference DBR is much wider than the stop band width of the low-contrast DBR.

SAMSUNG EX. 1031 - 12/30

Properties of DBRs can be calculated by the matrix method (Born and Wolf, 1989). The properties of DBRs have been analyzed in detail by Coldren and Corzine (1995), Yariv (1989), and Björk *et al.* (1995). Here, only a brief summary will be given.

Consider a distributed Bragg reflector consisting of m pairs of two dielectric, lossless materials with refractive indices $\bar{n}_l$ and $\bar{n}_h$. The thicknesses of the layers are assumed to be a quarter wave, i.e. $L_l = \lambda_{Bragg} / (4\bar{n}_l)$, and $L_h = \lambda_{Bragg} / (4\bar{n}_h)$. The period of the DBR is $L_l + L_h$. The reflectivity of a single interface is given by Fresnel's equation for normal incidence

$$r = \frac{\bar{n}_h - \bar{n}_l}{\bar{n}_h + \bar{n}_l} . \tag{10.12}$$

Multiple reflections at the interfaces of the DBR and constructive interference of the multiple reflected waves increase the reflectivity with increasing numbers of pairs. The reflectivity has a maximum at the Bragg wavelength λ_{Bragg}. The reflectivity at the Bragg wavelength of a DBR with m quarter-wave pairs is given by (Coldren and Corzine, 1995)

$$R_{DBR} = |r_{DBR}|^2 = \left[\frac{1 - (\bar{n}_l / \bar{n}_h)^{2m}}{1 + (\bar{n}_l / \bar{n}_h)^{2m}} \right]^2 . \tag{10.13}$$

The stop band of a DBR depends on the difference in refractive index of the two constituent materials, $\bar{n}_h - \bar{n}_l = \Delta\bar{n}$. The spectral width of the stop band is given by (Yariv, 1989)

$$\Delta\lambda_{stopband} = \frac{2\lambda_{Bragg}\,\Delta\bar{n}}{\pi\,\bar{n}_{eff}} \tag{10.14}$$

where $\bar{n}_{eff}$ is the effective refractive index of the DBR. For efficient operation of the LED, the stop band should be wider than the emission spectrum of the active region.

The effective refractive index of the DBR can be calculated by requiring the same optical path length normal to the layers for the DBR and an effective medium. The effective refractive index is then given by

$$\bar{n}_{eff} = 2\left(\frac{1}{\bar{n}_l} + \frac{1}{\bar{n}_h} \right)^{-1} . \tag{10.15}$$

For small index differences, i.e. $\Delta\bar{n} << \Delta\bar{n}_l$, the effective refractive index can be

SAMSUNG EX. 1031 - 13/30

approximated by

$$\bar{n}_{\text{eff}} = \frac{1}{2}\left(\bar{n}_{\text{l}} + \bar{n}_{\text{h}}\right) . \tag{10.16}$$

The optical wave penetrates into the DBR only by a finite number of quarter-wave pairs. That is, a finite number out of the total number of quarter-wave pairs are effectively reflecting the wave. The effective number of pairs "seen" by the wave electric field is given by (Coldren and Corzine, 1995)

$$m_{\text{eff}} \approx \frac{1}{2}\,\frac{\bar{n}_{\text{h}} + \bar{n}_{\text{l}}}{\bar{n}_{\text{h}} - \bar{n}_{\text{l}}}\,\tanh\left(2m\,\frac{\bar{n}_{\text{h}} - \bar{n}_{\text{l}}}{\bar{n}_{\text{h}} + \bar{n}_{\text{l}}}\right) . \tag{10.17}$$

For thick DBRs ($m \to \infty$), the tanh function approaches unity and one obtains

$$m_{\text{eff}} \approx \frac{1}{2}\,\frac{\bar{n}_{\text{h}} + \bar{n}_{\text{l}}}{\bar{n}_{\text{h}} - \bar{n}_{\text{l}}} . \tag{10.18}$$

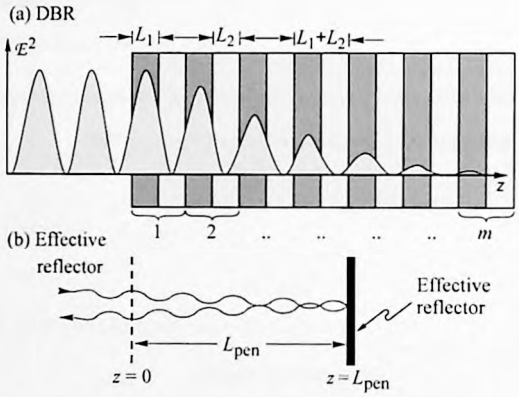

Fig. 10.9. Illustration of the DBR penetration depth. (a) DBR consisting of two materials with thickness L_1 and L_2. (b) Ideal (metallic) reflector displaced from the DBR surface by the penetration depth.

At the Bragg wavelength ($\lambda = \lambda_{\text{Bragg}}$), the phase change of the reflected wave is zero. In the vicinity of the Bragg wavelength ($\lambda \approx \lambda_{\text{Bragg}}$), the phase of the reflected wave changes *linearly* with wavelength. It is therefore possible to approximate a DBR with a metal-like mirror located a distance L_{pen} behind the first dielectric interface, as shown in Fig. 10.9. The reflection of the DBR can thus be expressed as

SAMSUNG EX. 1031 - 14/30

$$r_{\mathrm{DBR}} \approx \left| r_{\mathrm{DBR}} \right| \mathrm{e}^{-2\mathrm{i}\left(\beta - \beta_{\mathrm{Bragg}}\right) L_{\mathrm{pen}}} \tag{10.19}$$

where $\beta = 2\pi/\lambda$ is the average phase constant of the wave. The phase change at $z = 0$ (see Fig. 10.9) of the wave reflected by the metal mirror is given by

$$r_{\mathrm{metal}}\big|_{z=0} = \left| r_{\mathrm{metal}} \right| \mathrm{e}^{2\mathrm{i}\,(2\pi/\lambda)\,L_{\mathrm{pen}}} . \tag{10.20}$$

Equating the phase changes given by Eqs. (10.19) and (10.20) and using the phase changes of a DBR (Coldren and Corzine, 1995), the penetration depth is given by

$$L_{\mathrm{pen}} = \frac{L_1 + L_2}{4r} \tanh\left(2mr\right) . \tag{10.21}$$

For a large number of pairs ($m \to \infty$), the penetration depth is given by

$$L_{\mathrm{pen}} \approx \frac{L_1 + L_2}{4\,r} = \frac{\left(L_1 + L_2\right)}{4} \frac{\bar{n}_{\mathrm{h}} + \bar{n}_{\mathrm{l}}}{\bar{n}_{\mathrm{h}} - \bar{n}_{\mathrm{l}}} . \tag{10.22}$$

Comparison of Eqs. (10.22) and (10.18) yields that

$$L_{\mathrm{pen}} = (1/2)\, m_{\mathrm{eff}} \left(L_1 + L_2\right) . \tag{10.23}$$

The factor of (1/2) in Eq. (10.23) is due to the fact that m_{eff} applies to the effective number of periods seen by the *electric field*, whereas L_{pen} applies to the optical power. The optical power is equal to the square of the electric field and hence it penetrates half as far into the mirror. The effective length of a cavity consisting of two DBRs is thus given by the sum of the thickness of the center region plus the two penetration depths into the DBRs. The effective length of a cavity with DBRs is thus longer than the effective length of a cavity with metal mirrors.

The reflectivity of the DBR depends on the polar angle of incidence and on the wavelength. Although an analytic result can be obtained for the reflectivity of a DBR at the Bragg wavelength for normal incidence, the reflectivity of a DBR at an arbitrary wavelength and an arbitrary angle of incidence can only be calculated numerically. If light from an isotropic source is reflected by a DBR, the reflected intensity can be obtained by integration over all angles. The angle-integrated reflectance at a certain wavelength λ is then given by

SAMSUNG EX. 1031 - 15/30

$$R_{\text{int}}(\lambda) = \frac{\int_0^{\pi/2} R(\lambda,\Theta)\, 2\pi \sin\Theta \, d\Theta}{\int_0^{\pi/2} 2\pi \sin\Theta \, d\Theta} = \int_0^{\pi/2} R(\lambda,\Theta) \sin\Theta \, d\Theta \,. \tag{10.24}$$

The total light intensity reflected by the DBR is calculated by

$$I_r = \int_\lambda I_i(\lambda)\, R_{\text{int}}(\lambda)\, d\lambda \tag{10.25}$$

where $I_i(\lambda)$ is the emission intensity spectrum of the active region incident on the DBR and I_r is the intensity reflected by the DBR. For an isotropic emitter such as the active region of an LED, it can be assumed that the emission spectrum incident on the DBR is independent of the emission angle.

An efficient DBR will be optimized in such a way that it maximizes the intensity of the reflected light. In addition, the escape of the light reflected by the DBR from the LED die must be taken into account. Maximizing the LED extraction efficiency using a DBR is a complicated problem that cannot be solved analytically. *Ray tracing computer software* is used to maximize the extraction efficiency in LED structures with DBRs.

A priori, it is not clear that the use of conventional DBRs provides the best extraction efficiency. DBRs with layer thicknesses thinner or thicker than a quarter-wave should also be considered for maximization of the extraction efficiency. Such variable-thickness DBRs have a *lower reflectivity* but a *wider stop-band width* compared with quarter-wave DBRs. For active regions with broad emission spectra, such variable-period DBRs can be advantageous.

Ideally, the layers comprising the DBR are transparent. Layers of ***transparent DBRs*** have negligible absorption losses. However, transparent materials may not always be available so that *absorbing* materials must be used. Such ***absorbing DBRs*** have a maximum reflectivity of less than 100%, even if an infinite number of pairs are used.

An example of a partially absorbing Si/SiO_2 DBR is shown in Fig. 10.8. Silicon absorbs light for $\lambda < 1.1$ μm, i.e. for $h\nu > E_g$. However, the results shown in the figure demonstrate that very high reflectivities can be attained at 1.0 μm, where Si is absorbing. This is due to the high index contrast between Si and SiO_2.

Transparent and absorbing DBRs lattice matched to GaAs are used in the AlGaInP/GaAs material system. This material system is used for high-efficiency visible LEDs emitting at $\lambda > 550$ nm (green, yellow, amber, orange, and red). The properties of transparent and absorbing

SAMSUNG EX. 1031 - 16/30

DBRs used in this material system have been compiled by Kish and Fletcher (1997) and are summarized in Table 10.3. Inspection of the table reveals that the absorbing $Al_{0.5}In_{0.5}P/GaAs$ DBRs have the advantage of a high refractive index contrast. However, the absorbing nature of the DBR imposes an upper limit on the maximum reflectivity. High-contrast DBRs have a *wider* stop-band width. The transparent $Al_{0.5}In_{0.5}P/(AlGa)_{0.5}In_{0.5}P$ DBRs have the advantage of negligible optical losses. However, many pairs are needed to attain high reflectivity and the stop-band width is narrower than in high index-contrast DBRs.

Table 10.3. Properties of distributed Bragg reflector (DBR) materials used for visible and infrared LED applications. The DBRs marked as "lossy" are absorbing at the Bragg wavelength (data after Adachi, 1990; Adachi *et al.*, 1994; Kish and Fletcher, 1997; Babic *et al.*, 1999; Palik, 1998).

Material system	Bragg wavelength	$\bar{n}_{low}$	$\bar{n}_{high}$	$\Delta\bar{n}$	Transparency range
$Al_{0.5}In_{0.5}P/GaAs$	590 nm	3.13	3.90	0.87	> 870 nm (lossy)
$Al_{0.5}In_{0.5}P/Ga_{0.5}In_{0.5}P$	590 nm	3.13	3.74	0.61	> 649 nm (lossy)
$Al_{0.5}In_{0.5}P/(Al_{0.3}Ga_{0.7})_{0.5}In_{0.5}P$	615 nm	3.08	3.45	0.37	> 592 nm
$Al_{0.5}In_{0.5}P/(Al_{0.4}Ga_{0.6})_{0.5}In_{0.5}P$	590 nm	3.13	3.47	0.34	> 576 nm
$Al_{0.5}In_{0.5}P/(Al_{0.5}Ga_{0.5})_{0.5}In_{0.5}P$	570 nm	3.15	3.46	0.31	> 560 nm
AlAs/GaAs	900 nm	2.97	3.54	0.57	> 870 nm
SiO_2/Si	1300 nm	1.46	3.51	2.05	> 1106 nm

In practice, transparent layers are used at and near the top (epitaxial side) of the DBR whereas absorbing layers are used towards the bottom (substrate side) of the DBR. For DBRs used in manufactured AlGaInP/GaAs LEDs, each of the layers is different and optimized to keep the number of pairs low, the absorption low, and the reflectivity spectrum broad (Streubel, 2000).

Table 10.3 also shows properties of the AlAs/GaAs and the SiO_2/Si material systems. The SiO_2/Si material system is an example of a high index-contrast system. However, it cannot be used for current conduction due to the insulating nature of the SiO_2. The AlAs/GaAs material system is used in resonant-cavity LEDs and vertical-cavity surface-emitting lasers emitting in the range 880–980 nm.

A DBR that is resonant with the peak-emission wavelength, is not necessarily the optimum reflector for an absorbing substrate (AS) LED. Although a DBR has a high reflectivity for normal incidence, it rapidly decreases for off-normal angles of incidence. Assume that the angle of incidence is $\theta = 0°$ at normal incidence. Since the solid angle (per angle interval $d\theta$) increases

SAMSUNG EX. 1031 - 17/30

with angle θ according to a *sine* function, it is advantageous to shift the normal-incidence resonance wavelength of the DBR to wavelengths *longer* than the peak emission wavelength.

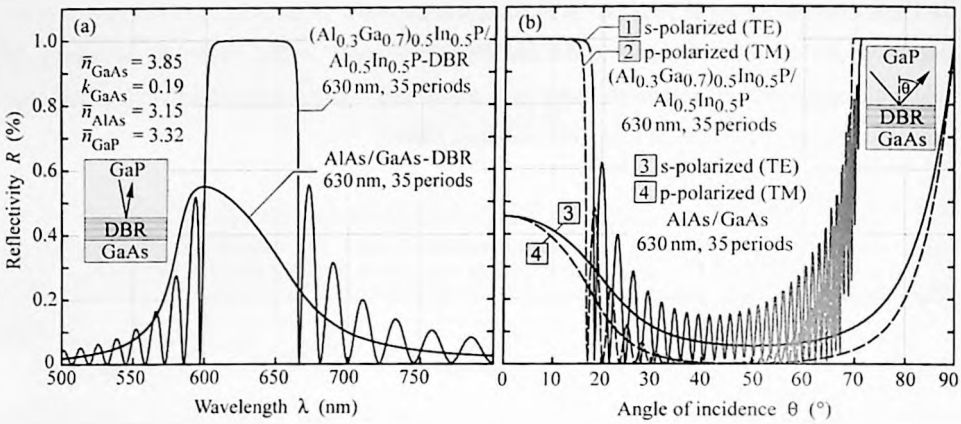

Fig. 10.10. Calculated reflectivity (inside the cladding GaP) versus (a) wavelength and (b) polar angle of a transparent AlGaInP/AlInP DBR and an absorbing AlAs/GaAs DBR.

The calculated reflectivities of a transparent and an absorbing DBR versus wavelength and polar angle of incidence are shown in Fig. 10.10. Whereas the DBR made of the transparent materials has a reflectivity close to 100% at the Bragg wavelength, the DBR that includes the absorbing GaAs layers has a maximum reflectivity of about 55%. This value cannot be increased by adding additional pairs to the DBR, because the limitation of the value lies in the absorptive nature of the DBR. The figure also shows the reflectivity of the DBRs versus the angle of incidence. Inspection of the figure reveals a major drawback of DBRs, namely the limitation of the high reflectivity band to small angles of incidence. For angles of incidence greater 20°, the reflectivity strongly decreases to assume values close to zero. Thus, for oblique angles of incidence (20° < θ < 70°), the DBR becomes non-reflective. The lack of reflectivity is a major loss mechanism in AlGaInP LEDs whose active layers are grown on top of a DBR that in turn is located on the absorbing GaAs substrate.

Next a formula will be derived that gives the critical angle, Θ_c, at which the reflectivity of a DBR strongly decreases. The structure of a DBR and the critical angle are illustrated in Fig. 10.11 (a) and (b), respectively. Note that the outside medium is a semiconductor with refractive index $\bar{n}_0$. For normal incidence (Θ = 0°), the Bragg condition is fulfilled at the Bragg

SAMSUNG EX. 1031 - 18/30

wavelength, λ_{Bragg}, which is located at the center of the high-reflectivity stop band. The Bragg wavelength shifts with angle of incidence, as shown in Fig. 10.11 (c). However, the *width* of the stop band does not depend on the angle of incidence as long as it is small. We can thus write the following condition for the critical angle Θ_c

$$\Delta\lambda_{Bragg} = \lambda_{Bragg}(\Theta = 0°) - \lambda_{Bragg}(\Theta_c) = \frac{1}{2}\Delta\lambda_{stop\ band} \,. \tag{10.26}$$

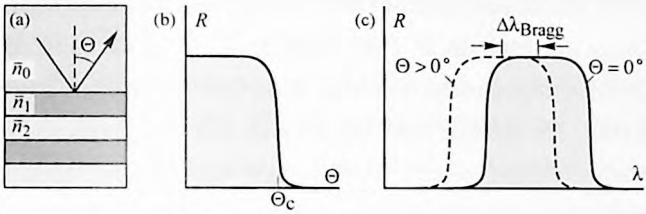

Fig. 10.11. (a) DBR stucture used in calculation. (b) Reflectivity versus angle of incidence and critical angle at which reflectivity decreases. (c) DBR reflectivity versus wavelength for two angles of incidence.

Using the expression for the angle-dependent Bragg wavelength and the expression for the width of the stop band given earlier in this chapter, one can write

$$\lambda_{Bragg}(\Theta = 0°)\left[1 - \cos\left(\frac{\bar{n}_0}{\bar{n}_1}\Theta_c\right)\right] = 2\,\lambda_{Bragg}(\Theta = 0°)\,\frac{\Delta\bar{n}}{\bar{n}_1 + \bar{n}_2}\,\frac{1}{\bar{n}_0} \,. \tag{10.27}$$

Dividing both sides of the equation by $\lambda_{Bragg}(\Theta = 0°)$ and solving the equation for Θ_c yields

$$\boxed{\Theta_c = \frac{\bar{n}_1}{\bar{n}_0}\arccos\left[1 - \left(\frac{2\Delta\bar{n}}{\bar{n}_1 + \bar{n}_2}\,\frac{1}{\bar{n}_0}\right)\right]} \,. \tag{10.28}$$

Using the approximation $\cos x \approx 1 - (1/2)\,x^2$ (valid near $x = 0$) and $\arccos x \approx [2\,(1 - x)]^{1/2}$ (valid near $x = 1$), the following approximation is obtained

$$\boxed{\Theta_c \approx \frac{\bar{n}_1}{\bar{n}_0}\sqrt{\frac{2}{\bar{n}_0}\,\frac{2\Delta\bar{n}}{\bar{n}_1 + \bar{n}_2}}} \,. \tag{10.29}$$

The equation shows that the critical angle strongly depends on the refractive index of the outside medium, $\bar{n}_0$, with $\Theta_c \propto (\bar{n}_0)^{-3/2}$. Thus the critical angle is small for outside media with a high refractive index. For this reason, it is difficult if not impossible to attain omnidirectional

SAMSUNG EX. 1031 - 19/30

reflection characteristics with a DBR if the outside medium is a high-index semiconductor.

As a numerical example, we consider an AlAs/GaAs DBR ($\bar{n}_{AlAs} = 3.0$; $\bar{n}_{GaAs} = 3.5$) with GaP as the outside medium ($\bar{n}_{GaP} = 3.1$). Insertion of these values in the equation for the critical angle yields $\Theta_c = 20.5°$, which is relatively close to normal incidence. Even high-contrast DBRs, such as SiO_2/Si DBRs, do not have omnidirectional characteristics if the outside medium is a high-index semiconductor.

Different strategies have been employed to optimize DBRs. Chiou *et al.* (2000) used a composite DBR in an AlGaInP LED, that is, two types of DBRs stacked on top of each other, namely a non-absorbing $(Al_{0.4}Ga_{0.6})_{0.5}In_{0.5}P/Al_{0.5}In_{0.5}P$ DBR resonant at the peak emission wavelength of 590 nm and an additional high-contrast absorbing AlAs/GaAs DBR. This DBR was located below the phosphide DBR. The arsenide DBR was resonant at a wavelength about 10% longer than the peak emission wavelength in order to reflect light incident at off-normal angles. The authors found a substantial improvement in light output with the composite DBR.

Non-periodic DBRs have a wider stop band and thereby a high reflectivity over a wider range of angles. To find optimum non-periodic DBR structures, numerical simulations and optimization procedures have been conducted (see, for example, Li *et al.*, 1999).

As shown by the calculation above, an increase in index contrast will provide a wider range of angles within which a high reflectivity is maintained. The use of such high-contrast DBRs in LEDs has been proposed by Chiou *et al.* (2003) who disclosed the use of an AlGaAs/Al_xO_y DBR in an LED. Al_2O_3 has a refractive index of about 1.75 whereas Al-rich AlGaAs has a refractive index of about 3.25 thus providing a large index contrast of $\Delta\bar{n} = 1.5$. The Al_xO_y layers of the DBR were fabricated from epitaxially grown AlAs by using an oxidation process that is performed in water vapor at temperatures of 400–450 °C. The Al_xO_y layers of the DBR are not conductive thus necessitating non-oxidized AlAs openings in the Al_xO_y layers, which provide a current path between substrate and active layers.

DBRs can have a high electrical resistance for current transport perpendicular to the layers. The resistance can pose a substantial problem in LED and laser structures, which manifests itself in a high forward voltage. Early experiments on VCSELs or vertical-cavity surface-emitting lasers (Jewell *et al.*, 1989; Koyama *et al.*, 1989) revealed forward voltages as high as 30.0 V (Jewell, 1992) and prevented these first devices from lasing in continuous-wave mode. The high resistance is caused by abrupt heterojunctions which pose barriers for carrier transport. Fortunately, heterojunction barriers can be completely eliminated by parabolic compositional grading (Schubert *et al.*, 1992a, 1992b). Such compositional grading is now routinely used in

SAMSUNG EX. 1031 - 20/30

DBRs so that the resistance issue of DBR heterojunctions no longer is a concern.

10.4 Omnidirectional reflectors

Electrically conductive high-reflectivity omnidirectional reflectors are highly desirable. With air as the outside medium, omnidirectional reflection characteristics can be demonstrated by using high-contrast DBRs. The high-contrast materials Si ($\bar{n} \approx 3.5$ at $\lambda = 1$ μm) and SiO_2 ($\bar{n} \approx 1.46$) are natural candidates for such ODRs. The optical properties of Si/SiO_2 distributed Bragg omnidirectional reflectors (DB-ODRs) and other material systems have been investigated (Chen *et al.*, 1999; Bruyant *et al.*, 2003).

Whereas omnidirectional TE reflectivity is readily obtained in DB-ODRs, the Brewster angle, at which the TM reflectivity decreases to zero, is an impediment in achieving omnidirectional characteristics for TM waves. An outside angle range of $0° \leq \Theta \leq 90°$ (in a low-index outside material such as air) results in an angle range $0° \leq \theta << 90°$ inside the material (i.e. inside the DBR). The inside range may not include the Brewster angle under which circumstances a DBR becomes omnidirectionally reflective.

Highly omnidirectional reflection characteristics were also obtained with DB-ODRs using polystyrene and Te layers (Fink *et al.*, 1998). Owing to the very large difference of the refractive indices, $\bar{n}_{polystyrene} = 1.8$ and $\bar{n}_{Te} = 5$, the interfacial Brewster angle θ_B is not accessible from light incident from air, resulting in a complete photonic bandgap in the wavelength range from 10 to 15 μm.

Another intriguing approach uses birefringent polymers with two different refractive indices parallel and vertical to the layer planes (Weber *et al.*, 2000). By adjusting the differences between the vertical and in-plane indices, the value of the Brewster angle can be controlled. Brewster angles up to 90° (grazing incidence) and even imaginary values are possible, resulting in a high reflectivity for TM-polarized light at virtually all angles of incidence.

Unfortunately the applicability of the above-mentioned DB-ODRs to LEDs is limited due to the insulating electrical characteristics of the constituent materials.

Metallic layers are capable of reflecting light over a wide range of wavelengths and incident angles with the high-reflectivity band being limited to frequencies below the plasma frequency of the free-electron gas (for historical references, see Drude, 1904; Lorentz 1909). However, electron oscillations induced by the incident light waves not only result in reflection but also in absorption caused by electron–phonon scattering. Thus, pure metal reflectors have significant

SAMSUNG EX. 1031 - 21/30

reflection losses, particularly when used on high-index materials.

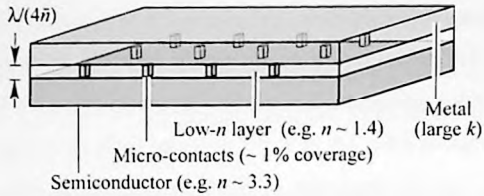

Fig. 10.12. Structure of omnidirectional reflector consisting of semiconductor, low-refractive index dielectric layer, and metal layer. The dielectric is perforated by an array of microcontacts providing electrical conductivity (after Gessmann *et al.*, 2003).

An electrically conductive reflector that has high-reflectivity and omnidirectional characteristics is shown in Fig. 10.12 (Schubert, 2001, 2004). It consists of three layers, a semiconductor, a dielectric layer, and a metal layer (triple-layer ODR). The dielectric layer is perforated by an array of microcontacts that provide electrical conductivity. The dielectric layer should have a refractive index as low as possible to provide a high index contrast to the semiconductor and the metal. The metal has a complex refractive index with a large extinction coefficient.

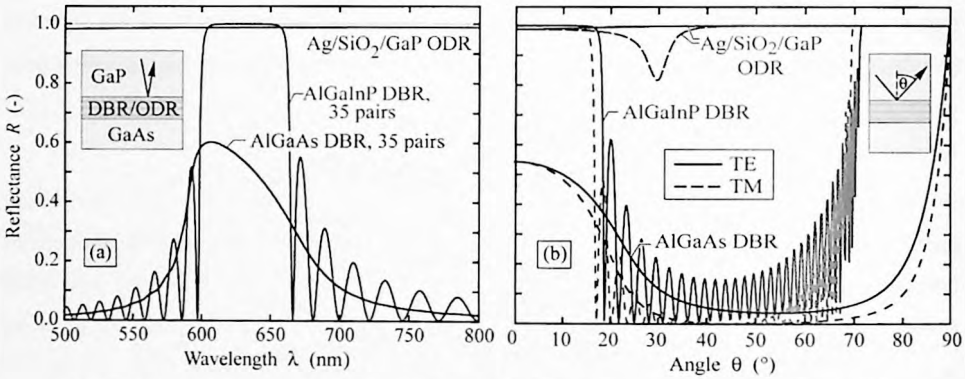

Fig. 10.13. (a) Calculated reflectance at normal-incidence versus wavelength and (b) reflectance versus angle of incidence for an omnidirectional reflector (ODR), a transparent AlGaInP/AlInP DBR, and an absorbing AlGaAs/GaAs DBR (after Gessmann *et al.*, 2003).

The reflectivity of the triple-layer ODR calculated by the matrix method is shown in Fig. 10.13 versus wavelength and versus angle along with the reflectivity of two DBRs (Gessmann *et al.*, 2003). The triple-layer ODR provides a broad reflectivity and omnidirectional characteristics. A small dip in the reflectivity is found for the TM wave at an incidence angle of

SAMSUNG EX. 1031 - 22/30

about 30° due to the reduced reflectivity of the semiconductor/dielectric interface at the Brewster angle. The angle-integrated reflectivity of the triple-layer ODR is very high and can exceed 99%.

At normal incidence ($\theta = 0$), the reflectivity of the triple-layer ODR can be calculated analytically and is given by

$$R_{\mathrm{ODR}} = \frac{\left[(\bar{n}_{\mathrm{s}} - \bar{n}_{\mathrm{li}})(\bar{n}_{\mathrm{li}} + \bar{n}_{\mathrm{m}}) + (\bar{n}_{\mathrm{s}} + \bar{n}_{\mathrm{li}})k_{\mathrm{m}}\right]^2 + \left[(\bar{n}_{\mathrm{s}} - \bar{n}_{\mathrm{li}})k_{\mathrm{m}} + (\bar{n}_{\mathrm{s}} + \bar{n}_{\mathrm{li}})(\bar{n}_{\mathrm{li}} - \bar{n}_{\mathrm{m}})\right]^2}{\left[(\bar{n}_{\mathrm{s}} + \bar{n}_{\mathrm{li}})(\bar{n}_{\mathrm{li}} + \bar{n}_{\mathrm{m}}) + (\bar{n}_{\mathrm{s}} - \bar{n}_{\mathrm{li}})k_{\mathrm{m}}\right]^2 + \left[(\bar{n}_{\mathrm{s}} + \bar{n}_{\mathrm{li}})k_{\mathrm{m}} + (\bar{n}_{\mathrm{s}} - \bar{n}_{\mathrm{li}})(\bar{n}_{\mathrm{li}} - \bar{n}_{\mathrm{m}})\right]^2} \quad (10.30)$$

where $\bar{n}_{\mathrm{li}}$ and $\bar{n}_{\mathrm{s}}$ are the refractive indices of the dielectric and semiconductor, respectively, and $N_{\mathrm{m}} = \bar{n}_{\mathrm{m}} + \mathrm{i}k_{\mathrm{m}}$ is the complex refractive index of the metal. The equation applies to a thickness of $\lambda_0/(4n_{\mathrm{li}})$ for the low-index dielectric layer, i.e. a quarter-wave layer. For an AlGaInP/SiO_2/Ag structure emitting at 630 nm, the equation yields a normal-incidence reflectivity $R_{\mathrm{ODR}}(\theta = 0)$ of 98.8% compared to a value of 96.1% for a structure without a dielectric layer.

650 nm AlGaInP LEDs using a triple-layer ODR have been demonstrated. The surface coverage of the microcontact array was 1%. The light-output power versus current characteristics of the ODR-LED and several reference devices are shown in Fig. 10.14 (Gessmann *et al.*, 2003). Comparison of the ODR-LED output characteristics with those of DBR-LEDs yields that the ODR-LED provides higher output powers.

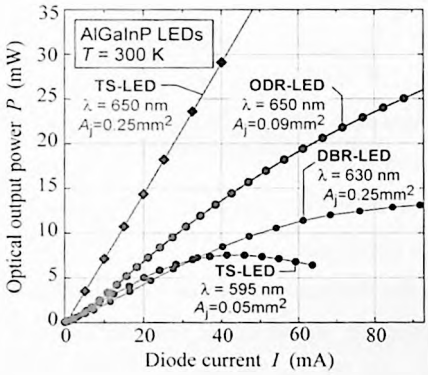

Fig. 10.14. Light-output power versus injection current of different types of LEDs. The ODR device has a higher output power than the DBR device (after Gessmann et al., 2003).

ODR-LEDs have also been demonstrated in the GaInN material system (Kim *et al.*, 2004). The ODR consisted of a RuO_2 ohmic contact to p-type GaN, a quarter-wave-thick SiO_2 low-index layer perforated by an array of microcontacts, and an Ag layer. Calculations predict a 98% angle-averaged reflectivity at $\lambda = 450$ nm for an GaN/SiO_2/Ag ODR, much higher than that for

SAMSUNG EX. 1031 - 23/30

an $Al_{0.25}Ga_{0.75}N/GaN$ distributed Bragg reflector (49%) and Ag (94%). It was shown that the $RuO_2/SiO_2/Ag$ ODR has a higher reflectivity than Ni/Au and even Ag reflectors, leading to a higher light extraction efficiency of the GaInN ODR-LED. The electrical properties of the ODR-LED were found to be comparable to those LEDs using conventional Ni/Au contacts. A comparison of the electrical and optical characteristics of the GaInN ODR device is shown in Fig. 10.15.

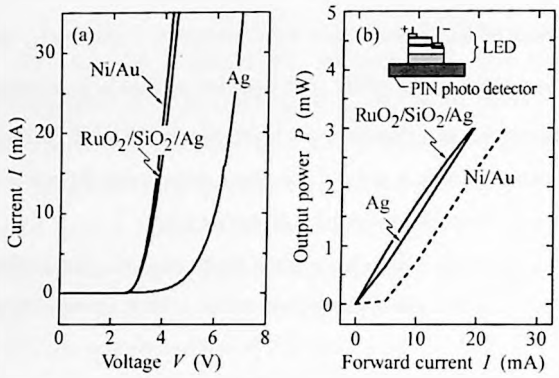

Fig. 10.15. Current–voltage and light-output-versus-current characteristics of a GaInN LED with a $GaInN/RuO_2/SiO_2/Ag$ omni-directional reflector (after Kim *et al.*, 2004).

10.5 Specular and diffuse reflectors

In ***specular reflectors***, the angle of the reflected light ray is equal to the angle of the incident light ray. Specular reflectors are thus deterministic, i.e. the angle of reflection is pre-determined by the angle of the incident light ray. ***Diffuse reflectors*** behave very differently, as shown in Fig. 10.16. The reflected intensity is distributed over a wide range of angles, independent of the incidence angle of the incoming ray. We will next discuss the properties of lambertian sources and lambertian reflectors and subsequently discuss implications for LEDs.

Lambertian surface sources are motivated by the frequently observed *experimental fact that the source radiance* (i.e. the optical power emitted per steradian per unit surface area of the source) *is a constant*, independent of the viewing angle. That is, the radiance and luminance of a lambertian source are independent of the viewing angle. The sun is the prime example of a lambertian source. As shown in Fig. 10.17(a), the sun's surface has the same brightness (luminance), irrespective of the viewing angle. That is, the brightness (luminance) is the same for, e.g., the normal-incidence viewing angle and an oblique-incidence viewing angle with respect to the sun's surface. For the same reason, the moon, shown in Fig. 10.17(b), can be

SAMSUNG EX. 1031 - 24/30

considered a good example of a lambertian reflector. Light-diffusing reflectors randomize the propagation direction of incoming photons and are referred to as ***diffuse or lambertian reflectors***.

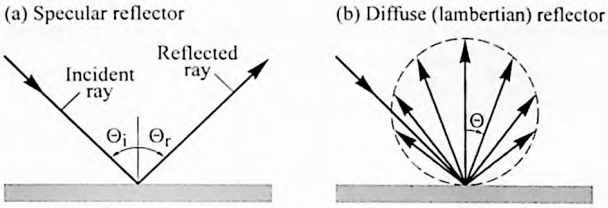

Fig. 10.16. Schematic of a specular and a diffuse (lambertian) reflector. The reflected power distribution of a lambertian reflector follows a $\cos\Theta$ dependence.

We now assume that a lambertian source has an intensity (i.e. optical power emitted per steradian) along the direction given by the angle Θ is given by

$$\boxed{I = I_n \cos\Theta} \tag{10.31}$$

where I_n is the intensity emitted normal to the reflector surface. The angular $\cos\Theta$ dependence of the equation is known as ***Lambert's cosine law***.

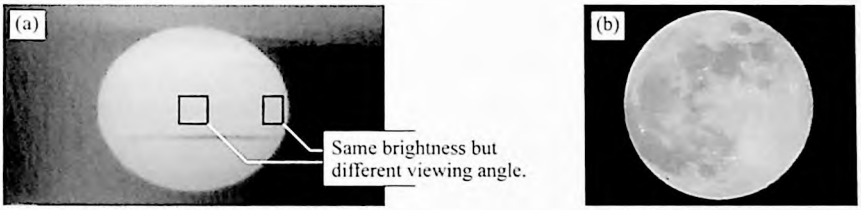

Fig. 10.17. (a) The sun's surface brightness is independent of viewing angle with respect to the sun's surface. It is a good example of a lambertian source. (b) The moon is a good example of a lambertian reflector.

Next, we will show that Lambert's cosine law results in a source luminance (or radiance, in radiometric units) that is *independent* of the viewing angle with respect to the source surface. Assume a lambertian surface source with area A. The projected area visible to an observer positioned at angle Θ is given by $A\cos\Theta$. Thus the luminance found by the observer is given by

$$\text{Luminance} = \frac{I_n A\cos\Theta}{A\cos\Theta} = I_n \tag{10.32}$$

SAMSUNG EX. 1031 - 25/30

where $A\cos\Theta$ is the surface area seen by the observer. Thus the luminance is constant, independent of the viewing angle. This fact is corroborated by the photographs shown in Fig. 10.17.

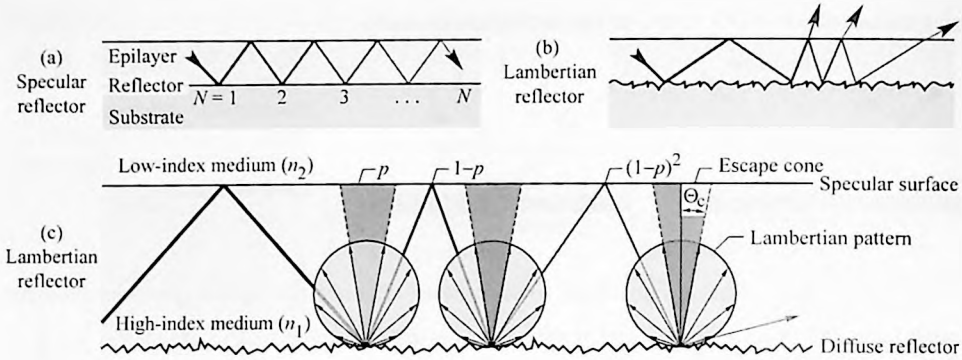

Fig. 10.18. (a) Optical ray, propagating in epilayer, guided by specular epilayer/substrate interface and epilayer/air interface. (b) and (c) Optical ray guided by lambertian reflector at epilayer/substrate interface and specular epilayer/air interface.

Light propagating in a layer clad by specular reflectors will be waveguided within the layer. However, light propagating in a layer clad by a lambertian reflector can be out-coupled into free space as shown in Fig. 10.18. As a lambertian reflector follows the $\cos\Theta$ dependence, the probability of reflected light falling into the escape cone defined by the angle Θ_c is given by

$$p = \frac{\int_0^{\Theta_c} I_n \cos\Theta \, 2\pi \sin\Theta \, d\Theta}{\int_0^{90°} I_n \cos\Theta \, 2\pi \sin\Theta \, d\Theta} = \frac{\int_0^{\Theta_c} \sin 2\Theta \, d\Theta}{\int_0^{90°} \sin 2\Theta \, d\Theta} = \frac{1-\cos 2\Theta_c}{2} . \qquad (10.33)$$

Using Snell's law ($\bar{n}_1 \sin\Theta_c = \bar{n}_2$, where $\bar{n}_1$ is the refractive index of the waveguide and $\bar{n}_1 > \bar{n}_2$), one obtains

$$p = \frac{1-\cos[2\arcsin(\bar{n}_2/\bar{n}_1)]}{2} = \left(\frac{\bar{n}_2}{\bar{n}_1}\right)^2 . \qquad (10.34)$$

Assuming a lambertian reflector with unit reflectivity ($R = 1.0$), the light intensity inside the semiconductor decreases according to a geometric series. After N reflection events, the intensity of the light ray will have fallen to $(1-p)^N$. Defining N as the number of reflection events after

SAMSUNG EX. 1031 - 26/30

which the light intensity has decreased to 1/e, we can write the equation

$$(1-p)^N = 1/\mathrm{e} \,. \tag{10.35}$$

Solving the equation for N allows one to calculate the average number of reflection events before the light ray will escape into the free space surrounding the semiconductor. One obtains

$$N = -\left[\ln\left(1 - n_2^2/n_1^2\right)\right]^{-1} . \tag{10.36}$$

As an example, we consider $\bar{n}_1 = 2.5$ (GaN) and $\bar{n}_2 = 1$ (air) and obtain $N = 5.7$. That is, light escapes from the waveguide after about six diffuse reflection events. Thus the introduction of diffuse reflectors into LED structures is a fruitful strategy in attaining laterally scalable emitters that do not suffer from an efficiency penalty usually associated with the up-scaling of the LED chip dimension (Kim *et al.*, 2006).

Mechanical roughening of reflective surfaces generally results in a change from specular to diffuse reflection characteristics. Such reflective surfaces can be, e.g., metallic surfaces or dielectric surfaces. In addition, porous silica (optionally coated with a metal) is known to have diffuse reflection characteristics as multiple refraction, reflection, and scattering events at pore/silica interfaces randomize the photon propagation direction.

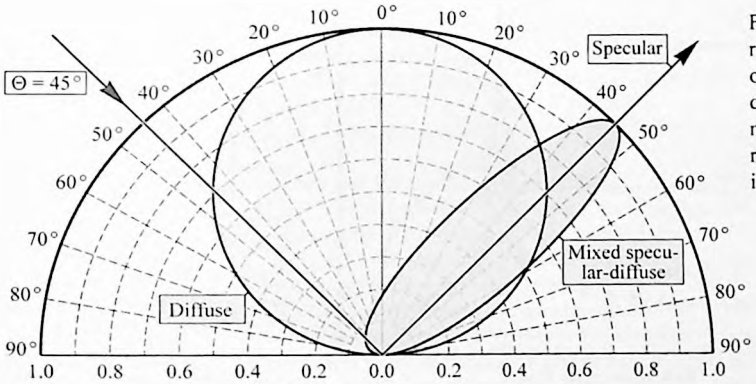

Fig. 10.19. Schematic reflection contour plots of a specular reflector, diffuse reflector, and a mixed specular-diffuse reflector for an angle of incidence of 45°.

The fabrication of *ideal* lambertian reflectors requires substantial roughness (greater than the wavelength of light, λ). Such ideal diffuse reflectors would have a reflection characteristic that is independent of the angle of incidence. Many real surface-textured reflectors have a mixed

SAMSUNG EX. 1031 - 27/30

specular-diffuse reflection characteristic with a *preferential* direction along the specular-reflection direction. Figure 10.19 shows the schematic reflection contour plots of a diffuse reflector, a mixed specular-diffuse reflector, and a specular reflector for an angle of incidence of 45°.

Figure 10.20 shows the measured reflected intensity versus reflection angle for a planar smooth Ag reflector and a surface-textured Ag reflector. The surface roughening was achieved by natural lithography using 700 nm diameter polystyrene spheres on the substrate, followed by ion-beam etching and Ag deposition. Inspection of the figure reveals a strong diffuse background for the textured reflector that is about two orders of magnitude higher than that of the planar Ag reflector. However, the textured reflector still exhibits a specular component. The relative strength of the diffuse and specular components of mixed specular-diffuse reflectors can be assessed quantitatively using the model developed by Xi *et al.* (2006). Using this model, it is found that the mixed specular-diffuse reflector, shown in Fig. 10.20, has a diffuse power ratio of $P_{diff}/(P_{spec} + P_{diff}) = 42.8\%$. The root-mean-square (rms) roughness of the partially diffuse reflector shown in Fig. 10.20 is 21.2 nm. By further increasing the rms roughness, diffusive power ratios of 100% can be attained.

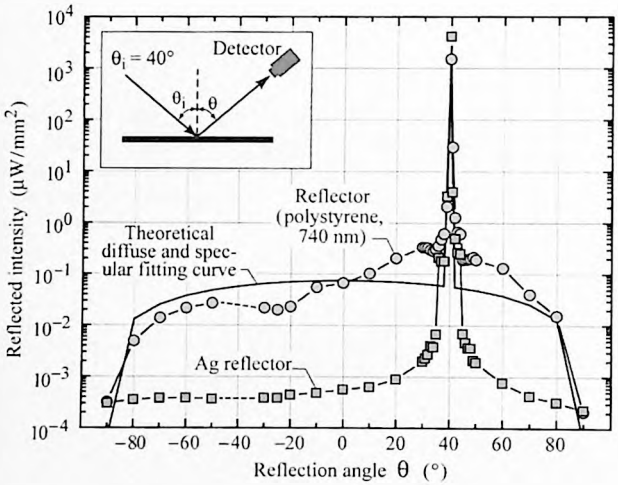

Smooth Ag reflector:
$P_{diff}/(P_{diff} + P_{spec}) < 1\%$

Textured Ag reflector:
$P_{diff}/(P_{diff} + P_{spec}) = 42.8\%$

Fig. 10.20. Reflected intensity versus angle for a smooth Ag reflector and a Ag reflector textured by using "natural lithography" with 700 nm diameter polystyrene spheres and subsequent ion-beam etching (after Xi *et al.*, 2006).

Exercise: ***Lambertian reflectors in LEDs***. Assume a lambertian reflector with reflectivity 1.0 that is incorporated in a lossless GaAs LED structure with refractive index of 3.5. Assume that the outside medium is air. Calculate the critical angle of the escape cone, the probability that a reflected light ray falls within the escape cone and the average number of reflection events before a photon escapes from the

SAMSUNG EX. 1031 - 28/30

high-index GaAs layer.

Solution: $\Theta_c = 16.6°$; $p = 8.2\%$; $N = 11.7$.

Would a hypothetical planar reflector that reflected light coming from any incoming direction towards the surface normal be useful? Is there a physical principle that prevents a reflector from reflecting light in such a way?

Answer: Although such a reflector would be very useful, such a reflector would unfortunately violate the ***conservation of radiance theorem*** (previously called the conservation of brightness theorem), which states that it is impossible to increase the radiance of light by a passive optical system beyond a value of L/n^2 where L is the radiance in vacuum and n is the refractive index of the medium in which the light propagates.

References

Adachi S. in *Properties of Gallium Arsenide* EMIS Datareview Ser. **2**, 513 INSPEC (IEE, New York, 1990)

Adachi S., Kato H., Moki A., and Ohtsuka K. "Refractive index of $(Al_xGa_{1-x})_{0.5}In_{0.5}P$ quaternary alloys" *J. Appl. Phys.* **75**, 478 (1994)

Babic D. I., Piprek L., and Bowers J. E. in *Vertical-Cavity Surface-Emitting Lasers* edited by C. W. Wilmsen, H. Temkin, and L. A. Coldren (Cambridge University Press, Cambridge, 1999)

Bell L. *The Telescope* this book discusses metal reflectors in a historical context; see pp. 220–227 (McGraw Hill, New York, 1922)

Björk G., Yamamoto Y., and Heitmann H. "Spontaneous emission control in semiconductor microcavities" in *Confined Electrons and Photons* edited by E. Burstein and C. Weisbuch (Plenum Press, New York, 1995)

Born M. and Wolf E. *Principles of Optics* 6th edition (Pergamon Press, New York, 1989)

Bruyant A., Lérondel G., Reece P. J., and Gal M. "All-silicon omnidirectional mirrors based on one-dimensional photonic crystals" *Appl. Phys. Lett.* **82**, 3227 (2003)

Chen K. M., Sparks A. W., Luan H.-C., Lim D. R., Wada K., and Kimerling L. C. "SiO_2/TiO_2 omnidirectional reflector and microcavity resonator via the sol-gel method" *Appl. Phys. Lett.* **75**, 3805 (1999)

Chiou S.-W., Lee C. P., Huang C. K., and Chen C. W. "Wide angle distributed Bragg reflectors for 590 nm amber AlGaInP light-emitting diodes" *J. Appl. Phys.* **87**, 2052 (2000)

Chiou S.-W., Chang H., Chen T.-P., and Chang C.-S. "Light emitting diodes and fabrication method thereof" US Patent 6,552,369 (2003)

Coldren L. A. and Corzine S. W. *Diode Lasers and Photonics Integrated Circuits* (John Wiley and Sons, New York, 1995)

Drude P. "Optische Eigenschaften und Elektronen Theorie I" ("Optical properties and electron theory I") *Annalen der Physik* **14**, 677 (1904); see also "Optische Eigenschaften und Elektronen Theorie II" ("Optical properties and electron theory II") *Annalen der Physik* **14**, 936 (1904)

Gessmann Th., Schubert E. F., Graff J. W., Streubel K., and Karnutsch C. "Omni-directionally reflective contacts for light-emitting diodes" *IEEE Electron. Dev. Lett.* **24**, 683 (2003)

Fink Y., Winn J. N., Fan S., Chen C., Michel J., Joannopoulos J. D., Thomas E. L. "A dielectric omnidirectional reflector" *Science* **282**, 1679 (1998)

Hecht J. *Understanding Fiber Optics* (Pearson Education, Upper Saddle River NJ, 2001)

Horng R. H., Wuu D. S., Wei S. C., Huang M. F., Chang K. H., Liu P. H., and Lin K. C. "AlGaInP/AuBe/glass light-emitting diodes fabricated by wafer bonding technology" *Appl. Phys. Lett.* **75**, 154 (1999a)

Horng R. H., Wuu D. S., Wei S. C., Tseng C. Y., Huang M. F., Chang K. H., Liu P. H., and Lin K. C. "AlGaInP light-emitting diodes with mirror substrates fabricated by wafer bonding" *Appl. Phys. Lett.* **75**, 3054 (1999b)

Jewell J. L., Huang K. F., Tai K., Lee Y. H., Fischer R. J., McCall S. L., and Cho A. Y. "Vertical cavity single quantum well laser" *Appl. Phys. Lett.* **55**, 424 (1989)

SAMSUNG EX. 1031 - 29/30

Jewell J. L. personal communication (1992)

Kato T., Susawa H., Hirotani M., Saka T., Ohashi Y., Shichi E., and Shibata S. "GaAs/GaAlAs surface emitting IR LED with Bragg reflector grown by MOCVD" *J. Cryst. Growth* **107**, 832 (1991)

Kepler J. *Dioptrice* (1611)

Kim J. K., Gessmann T., Luo H., and Schubert E. F. "GaInN light-emitting diodes with $RuO_2/SiO_2/Ag$ omni-directional reflector" *Appl. Phys. Lett.* **84**, 4508 (2004)

Kim J. K., Luo H., Xi Y., Shah J. M., Gessmann T., and Schubert E. F. "Light extraction in GaInN light-emitting diodes using diffuse omnidirectional reflectors" *Journal of the Electrochemical Society* **153**, G105 (2006)

Kish F. A. and Fletcher R. M. "AlGaInP light-emitting diodes" in *High Brightness Light-Emitting Diodes* edited by G. B. Stringfellow and M. G. Craford, Semiconductors and Semimetals **48** (Academic, San Diego, 1997)

Koyama F., Kinoshita S., and Iga K. "Room temperature continuous wave lasing characteristics of a GaAs vertical-cavity surface-emitting laser" *Appl. Phys. Lett.* **55**, 221 (1989)

Li H., Gu G., Chen H., and Zhu S. "Disordered dielectric high reflectors with broadband from visible to infrared" *Appl. Phys. Lett.* **74**, 3260 (1999)

Lorentz H. A. *The Theory of Electrons and its Applications to the Phenomena of Light and Radiant Heat* (Teubner, Leipzig, Germany, 1909)

Margalith T., Buchinsky O., Cohen D. A., Abare A. C., Hansen M., DenBaars S. P., and Coldren L. A. "Indium tin oxide contacts to gallium nitride optoelectronic devices" *Appl. Phys. Lett.* **74**, 3930 (1999)

McCall S. L., Levi A. F. J., Slusher R. E., Pearton S. J., and Logan R. A. "Whispering-gallery mode microdisk lasers" *Appl. Phys. Lett.* **60**, 289 (1992)

Mergel D., Stass W., Ehl G., and Barthel D. "Oxygen incorporation in thin films of In_2O_3:Sn prepared by radio frequency sputtering" *J. Appl. Phys.* **88**, 2437 (2000)

Palik E. D. *Handbook of Optical Constants of Solids* (Academic Press, San Diego, 1998)

Ray S., Banerjee R., Basu N., Batabyal A. K., and Barua A. K. "Properties of tin doped indium oxide thin films prepared by magnetron sputtering" *J. Appl. Phys.* **54**, 3497 (1983)

Schubert E. F., Tu L.-W., Zydzik G. J., Kopf R. F., Benvenuti A., and Pinto M. R. "Elimination of heterojunction band discontinuities by modulation doping" *Appl. Phys. Lett.* **60**, 466 (1992a)

Schubert E. F., Tu L.-W., and Zydzik G. J. "Elimination of heterojunction band discontinuities" US Patent No. 5,170,407 (1992b)

Schubert E. F. "Light-emitting diode with omni-directional reflector" US Patent application 60/339,335 (2001)

Schubert E. F. "Light-emitting diode with omni-directional reflector" US Patent 6,784,462; issued Aug. 31 (2004)

Sheu J. K., Su Y. K., Chi G. C., Jou M. J., and Chang C. M. " Effects of thermal annealing on the indium tin oxide Schottky contacts of n-GaN" *Appl. Phys. Lett.* **72**, 3317 (1998)

Shin J. H., Shin S. H., Park J. I., and Kim H. H. "Properties of dc magnetron sputtered indium tin oxide films on polymeric substrates at room temperature" *J. Appl. Phys.* **89**, 5199 (2001)

Smith G. M., Forbes D. V., Coleman J. J., and Verdeyen J. T. "Optical properties of reactive ion etched corner reflector strained-layer InGaAs–GaAs–AlGaAs quantum-well lasers" *IEEE Photonics Technol. Lett.* **5**, 873 (1993)

Streubel K., personal communication (2000)

Tu L. W., Schubert E. F., Kopf R. F., Zydzik G. J., Hong M., Chu S. N. G., and Mannaerts J. P. "Vertical cavity surface emitting lasers with semitransparent metallic mirrors and high quantum efficiencies" *Appl. Phys. Lett.* **57**, 2045 (1990)

Weber M. F., Stover C. A., Gilbert L. R., Nevitt T. J., and Ouderkirk A. J. "Giant birefringent optics in multilayer polymer mirrors" *Science* **287**, 2451 (2000)

Xi Y., Kim J. K., Mont F., Gessmann Th., Luo H., and Schubert E. F. "Quantitative assessment of diffusivity and specularity of surface-textured reflectors for light extraction in light-emitting diodes" manuscript in preparation (2006)

Yariv A. *Quantum Electronics* 3rd edition (John Wiley and Sons, New York, 1989)

SAMSUNG EX. 1031 - 30/30